Carbohydrate Polymers 333 (2024) 121966

Contents lists available at ScienceDirect

Carbohydrate Polymers

journal homepage: www.elsevier.com/locate/carbpol

Mechanically robust, thermal insulating sustainable foams fully derived from bamboo fibers through high temperature drying

Xin Li [a,b], Tuhua Zhong [b,c,*], Yunyan Xiao [a], Haitao Cheng [b,c,*], Hong Chen [a,**]

[a] College of Furnishings and Industrial Design and Co-Innovation Center of Efficient Processing and Utilization of Forest Resources, Nanjing Forestry University, Nanjing 210037, China
[b] International Centre for Bamboo and Rattan, Beijing 100102, China
[c] NFGA/Beijing Key Laboratory for Bamboo & Rattan Science and Technology, National Forestry and Grassland Administration, Beijing 100102, China

ARTICLE INFO

Keywords:
Bamboo fiber foam
High solid fibrillated cellulose
Thermal insulation
Mechanical performance

ABSTRACT

The development of lignocellulosic foams has been gaining momentum due to their sustainability and biodegradability. However, lignocellulosic foams often have low preparation efficiency and poor mechanical properties, especially compression performance. Here, we constructed mechanically robust and thermal insulating cellulosic foams through high-temperature drying, in which all bamboo-sourced lignin-containing pulp fibers (LPF) and steam explosion fibers (SEF) were chosen as a skeleton and high solid fibrillated cellulose (HSFC) as a binder. This study aimed to investigate the effects of the characteristics of bamboo fibers and the HSFC addition on the formation, and mechanical- and thermal insulation performances of the resulting foams. The HSFC incorporation endowed the foams with excellent mechanical performance, the stress at 10 % strain and compressive modulus were 0.29 MPa and 4.4 MPa, respectively, which were 10-fold and 44-fold compared to LPF foam without HSFC. The LPF/HSFC possessed excellent energy absorption capacity (170 kJ/m^3 under 40 % strain) as well as good thermal insulating performance (0.054 W/(m·K)). The LPF/HSFC foam with a much more homogeneous cellular structure outperformed the SEF/HSFC foam. This work suggests that the developed bamboo fiber foams hold promise for use in protective packaging and thermal insulation applications.

1. Introduction

Plastic foams are prevalent in our daily lives, such as insulation materials in buildings and packaging, and shock absorption materials in transportation, because they have impressive features such as lightweight, thermal insulation, and energy absorption capabilities, *etc.* (Wu et al., 2021). Most plastic foams are made from petrochemical-based feedstocks, particularly including polyurethane (PU), expanded polystyrene (EPS), *etc.* (Ates, Karadag, Eker, & Eker, 2022; Zhao et al., 2022). It usually takes hundreds of years for such plastic waste to decompose, giving rise to mounting environmental burdens as more and more plastic waste is dumped into the environment (Blettler, Ulla, Rabuffetti, & Garello, 2017; Li et al., 2021; Turner & Lau, 2016). Even though these petrochemical plastics can be broken down into tiny microplastics in the long term, it was found the ensuing tiny microplastics pose serious threats to human health and the ecosystems (Vethaak & Legler, 2021). In recent years, the development of environmentally friendly foams, particularly deriving from natural sources, has gained growing momentum, which is aimed at replacing some petrochemical-based foams.

Among a variety of natural feedstocks, cellulose is the most abundant biopolymer on Earth (Moon, Martini, Nairn, Simonsen, & Youngblood, 2011). There has been extensive research on lignocellulosic foams (Chen et al., 2022; Hafez & Tajvidi, 2021; Zhu et al., 2022). Lignocellulosic fibers have been attempted to be directly used to manufacture foams, but their structures are loose and easily broken apart due to a lack of structural integrity (Zhu et al., 2022). To address this issue, pretreatments or the use of synthetic or natural additives have been attempted to strengthen the mechanical properties of lignocellulosic foam. For example, chemi-thermomechnical pulp (CTMP) was prefibrillated by disc milling to in-situ generate sub-microfibrils to extend the hydrogen bonding after ambient drying to enhance the interaction between adjacent fibers, thereby endowing its structural integrity (Zhu

* Corresponding authors at: International Centre for Bamboo and Rattan, Beijing 100102, China; NFGA/Beijing Key Laboratory for Bamboo & Rattan Science and Technology, National Forestry and Grassland Administration, Beijing 100102, China.
** Corresponding author.
E-mail addresses: zhongth@icbr.ac.cn (T. Zhong), htcheng@icbr.ac.cn (H. Cheng), chenhong@njfu.edu.cn (H. Chen).

https://doi.org/10.1016/j.carbpol.2024.121966
Received 13 December 2023; Received in revised form 2 February 2024; Accepted 16 February 2024
Available online 19 February 2024

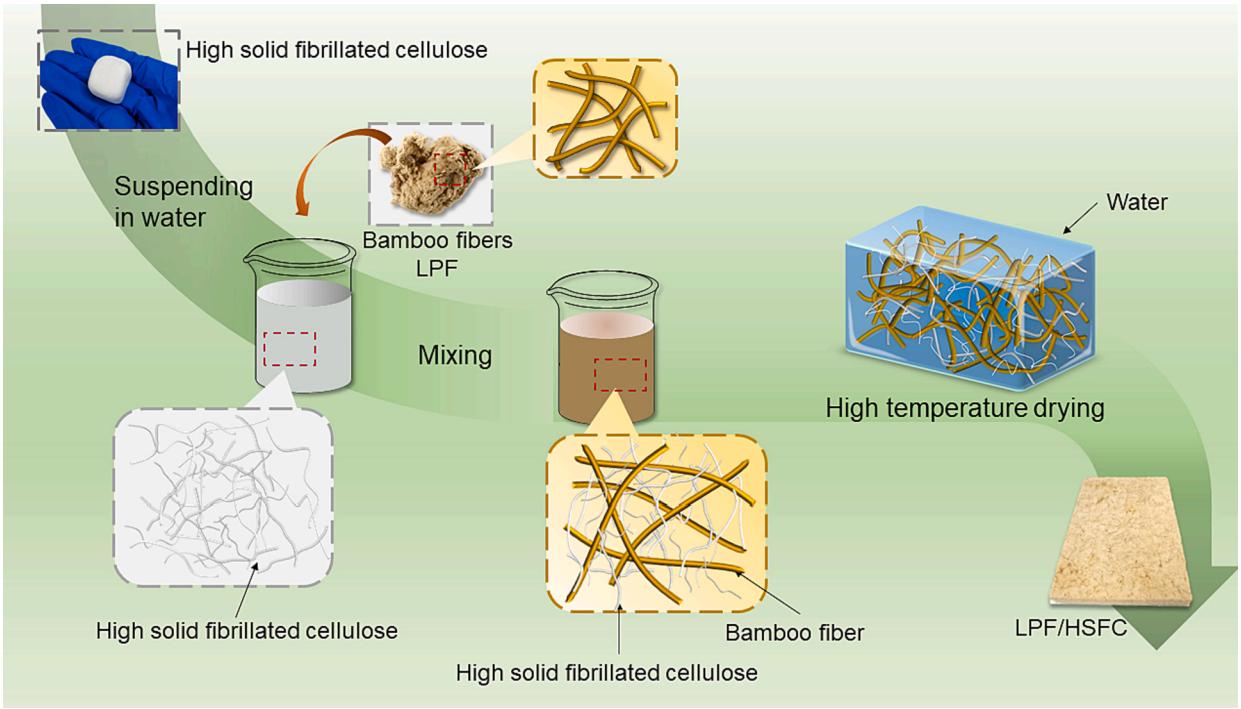

Fig. 1. Schematic diagram of the fabrication process of bamboo fiber foams made of bamboo fibers LPF and HSFC.

et al., 2022). If pretreatments are not involved, chemical cross-linkers such as citric acids, diphenyl diisocyanate (MDI), or polyamidoamine epichlorohydrin are often used to strengthen the mechanical properties of lignocellulosic foams (Ferreira, Cranston, & Rezende, 2020; Liu, Lu, Xiao, Heydarifard, & Wang, 2017; Malekzadeh, Md Zaid, & Bele, 2021; Wu et al., 2022). Another commonly used approach is to incorporate nanocellulose as a natural "adhesive" into lignocellulosic fibers to construct lignocellulosic foams (Hafez & Tajvidi, 2021; Sun et al., 2023; Sun, Chu, Wu, & Xiao, 2021).

Nanocellulose is an ideal natural "binder" used in lignocellulosic foam manufacture. However, nanocellulose still faces an imperative issue such as its high production cost arising from high water/energy consumption during the extraction process, which hinders its scale-up applications in commercial products and needs to be addressed. Our previously developed high-consistency mechano-enzymatic fibrillation approach was able to produce high-solid fibrillated cellulose (HSFC) (solid content = 27 %), in which most micro-and nanofibrils could be readily obtained in a large quantity, thus greatly reducing water/energy consumption (Pere et al., 2020; Wang et al., 2022). We thought HSFC could serve as a promising reinforcing material to combine with relatively coarse lignocellulosic fibers to construct sustainable foams in this study.

There are many approaches to fabricating lignocellulosic foams, mainly including ice templating/freeze drying, solvent exchange/supercritical drying, microwave radiation, and bubble templating/air drying (Gupta, Singh, Agrawal, & Maji, 2018; Jiménez-Saelices, Seantier, Cathala, & Grohens, 2017; Ma et al., 2021; Wang et al., 2016). Freeze-drying and supercritical drying processes are often time-consuming and energy-intensive, and expensive facilities are usually involved, thus hindering their scale-up production (Chen et al., 2022). There is no doubt that bubble templating/air drying is an environmentally friendly, less energy-intensive method, and has the potential to be scaled up for the fabrication of lignocellulose foams (Chen et al., 2022; Jaxel, Markevicius, Rigacci, & Budtova, 2017; Zhu et al., 2022), but now the drying time is still too long, usually longer than 6 h at 75°C or 72 h at room temperature (Markevicius, Ladj, Niemeyer, Budtova, & Rigacci, 2017; Zhu et al., 2023). Thermal drying at high temperatures (>100 °C, for example at 200 °C) might be a relatively fast and efficient way to manufacture lignocellulosic foams.

Here, we proposed to use high-temperature drying to produce bamboo fiber foams made of bamboo fibers and HSFC without any external foaming agents or chemical cross-linkers, in which the HSFC was also prepared using bamboo fibers as raw material in a green fashion. We hypothesized that the "paste-like" mixture of bamboo fibers and HSFC was mixed and then heated at 200°C for 1.5 h, triggering water inside to instantaneously evaporate and giving rise to internal vapor pressure to resist the capillary-force driven structural collapse of the preformed three dimensional (3D) structure to some extent, creating the cellular structure; as the water evaporated, HSFC with high specific surface areas in this system was able to form a "film bridge" to bond adjacent bamboo fibers, thus enhancing interaction among fibers and imparting its structural integrity, and eventually leading to mechanical robustness of lignocellulosic foams in a fast and efficient production way. The developed foams were intended for use in thermal insulating or protective packaging materials. Two different types of bamboo fibers and the HSFC addition were investigated regarding their effects on the internal structure and material properties of the resulting foams in terms of formation, mechanical performance, thermal insulation, and thermal stability.

2. Materials and methods

2.1. Materials

The five-year-old moso bamboo (*Phyllostachys heterocycla*) was collected from Zhejiang Province, China. The bamboo-sourced lignin-containing pulp fibers (LPF) were kindly provided by Sichuan Huanlong New Material, China. Bleached kraft bamboo pulp (BKBP) was kindly provided by Sichuan Yongfeng Pulp and Paper, China. Cellulase (CTec3, the enzyme activity: 9.5 FPU/mL) was from Novozymes (Novozymes, China). Glacial acetic acid (Analytical reagent, 99.5 %), and sodium acetate (Analytical reagent, 99 %) were purchased from Macklin, China. Expanded polystyrene (EPS) foam was from Beijing Zhiheng Horticultural Franchise Store, China. Polyurethane (PU) foam was from

Zhenjiang Huajiang Science and Technology, China. Polypropylene (PP) foam was from Kunshan Starting Line Packaging Materials, China.

2.2. The preparation of steam explosion fibers (SEF)

Bamboo strips with a size of 50 mm × 20 mm × 2 mm were soaked in water until saturated and then underwent splitting by roller twice. Subsequently, the pretreated bamboo strips (100 g) and water (50 g) were loaded into a steam explosion device (QBS-80, Qingzheng Ecological Technology, China), with an explosion pressure of 2.2 MPa and a duration of 4 min. Upon the predefined time, the pressure was released, the materials inside the chamber were sprayed into the discharging device, and bamboo fibers were collected after two repeated explosion processes.

2.3. The preparation of high solid fibrillated cellulose (HSFC)

The HSFC product was prepared according to our previously developed procedures (Wang et al., 2022). Briefly, the enzymes in acetate buffer (pH = 5) were sprayed onto shredded pulp fibers. The mechano-enzymatic treatment of bamboo pulp fibers was carried out for 8 h in a mixer with two sigma blades (NH-1, Rugao Guanchen Machinery Factory, China). The temperature of the reactor was set at 50 ± 3 °C. Upon the completion of reaction time, the enzymes were deactivated with 90 °C boiling water, and then the samples were washed thoroughly with boiling water through filtration, and high solid fibrillated cellulose (HSFC) was obtained and stored in the refrigerator for use.

2.4. The fabrication of bamboo fiber foams

The foam comprising bamboo fiber and HSFC at a weight ratio of 6:4 was prepared. As shown in Fig. 1, the bamboo fibers LPF and HSFC were mixed in water to form a "paste-like" mixture. Subsequently, the LPF and HSFC mixture were heated at 200 °C for 1.5 h to obtain bamboo fiber foam. Based on two different types of bamboo fibers (LPF and SEF), the resulting foams comprising bamboo fibers and HSFC were simply coded as LPF/HSFC foam and SEF/HSFC foam, respectively. The bamboo fiber foams without HSFC were also prepared as control following the same procedures described above, the control ones were coded as LPF foam and SEF foam, respectively.

2.5. Characterizations

2.5.1. Scanning electron microscope (SEM) observation

The morphology of bamboo fibers and microstructure of bamboo fiber foams were observed by scanning electron microscopy (SEM, GeminiSEM360, Zeiss, Germany). Before SEM imaging, the samples were coated with gold using an ion sputter coater.

2.5.2. Chemical composition analysis

The chemical compositions of bamboo fibers were determined according to the procedures described in the protocol NREL/TP-510-42618 (Sluiter et al., 2008). The content of acid-soluble lignin was measured by an ultraviolet spectrophotometer (UV-1800, ESM, China) at the wavelength of 205 nm. The relative lignin content was determined by drying the solid at (105 ± 3) °C in a muffle furnace (CR7, China) (Wu et al., 2023). The measurement was performed in triplicate.

2.5.3. Fourier Transform Infrared (FTIR) analysis

The FTIR spectra of bamboo fibers were recorded with an infrared spectrometer (Thermo Fisher Scientific, USA) scanning from 400 to 4000 cm^{-1} with a resolution of 4 cm^{-1}, and the scanning times of 64. The fibers were mixed with KBr at a weight ratio of 1:100 and then pressed into a pellet.

2.5.4. X-ray diffraction (XRD) measurement

The diffractograms of bamboo fibers were measured by X-ray diffractometer (X PERTPRO-30X, Philipp, Netherlands) using CuKα (λ = 0.154 nm) with a test range of 5° ~ 45° and a test speed of 10°/min. The crystallinity index (CrI) was calculated according to Segal's formula (Segal, Creely, Martin Jr, & Conrad, 1959).

$$CrI = \frac{I_{200} - I_{am}}{I_{200}} \times 100\% \quad (1)$$

where *CrI* is crystallinity index (%), I_{200} represents the diffraction intensity of the 200 crystalline plane (2θ = 22.2°), and I_{am} represents the diffraction intensity of the amorphous region (2θ = 18.0°).

2.5.5. Atomic Force Microscopy (AFM) observation

The morphology of HSFC was observed with atomic force microscopy (Dimension Icon, Bruker, Germany). Before observation, a drop of diluted HSFC suspension (0.001 %) was dropped on a clean mica sheet surface and air-dried. The images were taken in tap mode on an aluminum-coated silicon cantilever with a probe radius of 8 nm, a scan speed of 0.5 Hz, and a resonance frequency between 300 kHz and 380 kHz.

2.5.6. Micro-CT observation

The bamboo fiber foams with a dimension of 10 mm × 10 mm × 8 mm were scanned by micro-computed tomography (micro-CT) (SkyScan 2214, Bruker, Belgium) with a tube voltage of 80 kV, a tube current of 50 μA, a scanning time of 2 h, and a resolution of 6.60 μm. A threshold segmentation method was used to extract the voids in the interface between bamboo fibers and HSFC, and a 3D model was reconstructed. Then porosity was calculated by modeling through Avizo software using commands "Interactive Thresholding" and "Volume Rendering Settings".

2.5.7. Compression test

The compression test of bamboo fiber foams with a dimension of 20 mm × 20 mm × 15 mm was carried out using the micro-mechanical testing machine (Instron 5848, Instron, UK), with a load sensor was 2000 N, and a compression speed of 1 mm/min. The compressive modulus was calculated based on the initial linear regime of the stress-strain response under 10 % strain. The maximum compression deformation was set to 70 % strain. The test was conducted at a temperature of 25 °C and a relative humidity of 60 %. The tests for each sample were performed in triplicate. A compression test of commercial PU foam was carried out as a control. The energy absorption capacity was determined as the area under the curves from 0 % to 40 % strain. The breakage test was carried out using long strip samples with a dimension of 76 mm × 20 mm × 8 mm. The long bamboo fiber foams were placed on two solid supports with 6 cm spacing, and a 500 g weight was placed on top of the stick.

2.5.8. Thermal conductivity measurements

The thermal conductivity of bamboo fiber foams with a dimension of 20 mm × 20 mm × 15 mm was measured by a thermal conductivity tester (Tci, C-Therm Technologies Ltd., Canada). The testing average temperature is set at 25 °C, with a temperature difference of 30 °C between the cold platen and hot platen. The measurements were performed in triplicate. The thermal conductivity of commercial PU foam was measured as a control. Infrared (IR) imaging was taken using an IR Thermal Imaging camera (HM-TPH21Pro-3AQF, Hikmicro, China), and the experiments were conducted on a hot plate with a constant temperature.

2.5.9. Density

The apparent density (ρ) of bamboo fiber foams (20 mm × 20 mm × 10 mm) was calculated by equation.

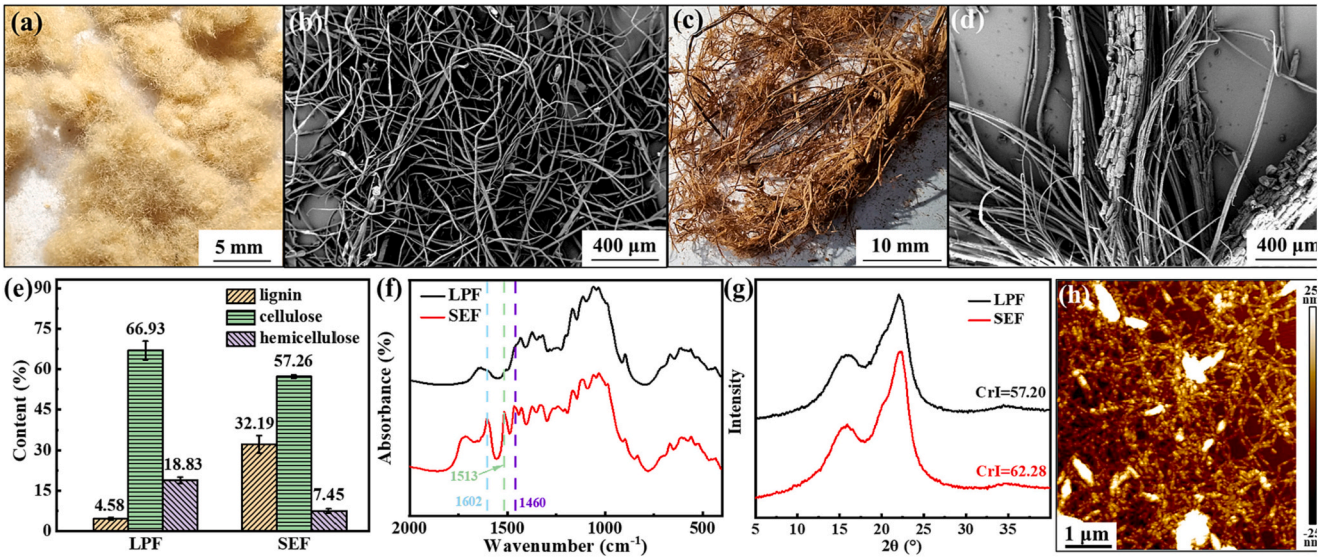

Fig. 2. Photograph (a) of the LPF and the corresponding SEM image (b) of the morphology; photograph (c) of the SEF and the corresponding SEM image (d) of the morphology; (e) chemical compositions, (f) FTIR spectra, (g) XRD patterns of bamboo fibers and (h) AFM image of the HSFC product.

$$\rho = \frac{m}{V} \tag{2}$$

where m and V is the weight and volume of bamboo fiber foams, respectively.

2.5.10. Thermogravimetric (TG) analysis

The thermal stability of bamboo fiber foams was assessed with a synchronous thermogravimetric (TG) analyzer (TGA 4000, PerkinElmer, USA) in a nitrogen atmosphere with flow rates of 20 mL/min. The temperature ramped up from 30 to 600 °C, with a heating rate of 10 °C/min. The measurement was performed in triplicate.

2.5.11. Scene simulation

Six planes of LPF/HSFC foams were used to build a model bungalow building. The hot scenario was demonstrated using a heating table (75 °C), and the cold scenario was demonstrated using ice cubes (0 °C). The PU foam bungalow building model was also built and tested as a control.

3. Results and discussion

3.1. Characteristics of bamboo fibers and high solid nanocellulose used for the bamboo fiber foam fabrication

As shown in Fig. 2a–d, fluffy LPF was much more uniform in size and

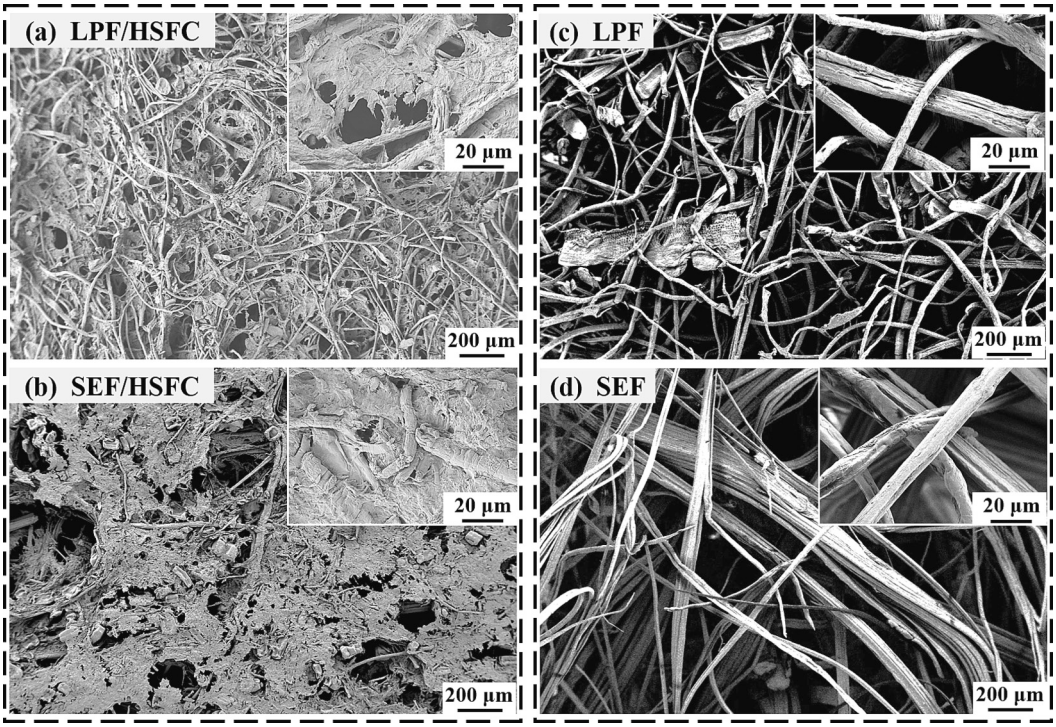

Fig. 3. SEM images of microstructure of bamboo fiber foams (a, LPF/HSFC; b, SEF/HSFC) and fiber foams without the HSFC (c, PF; d, SEF).

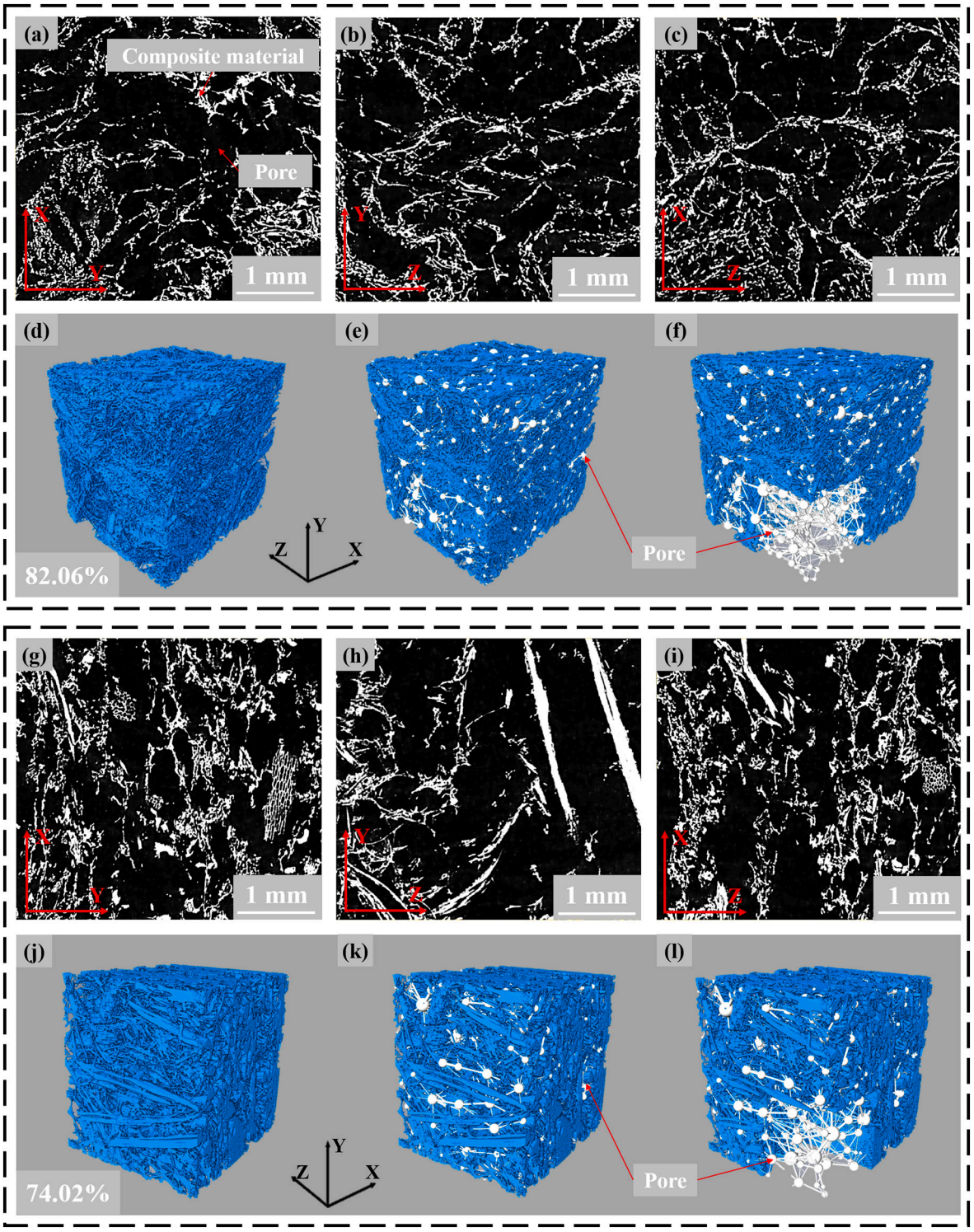

Fig. 4. Two-dimensional (2D) cross-sections (a–c: LPF/HSFC, g–i: SEF/HSFC) and three-dimensional (3D) reconstruction model of bamboo fiber foams (d–f: LPF/HSFC, j–l: SEF/HSFC) based on Micro-CT images: a rebuilt 3D porous structure (left), a 3D structure with pores filled with "white balls" simulating the actual pores inside the foams, (middle), a 3D structure with partial matrix removal exposing "white balls" which size varied depending on actual pore sizes.

shape compared to SEF. The average diameter of LPF was around 10.2 μm, and the size of SEF was 17.9 μm with a fraction of not completely fibrillated fiber bundles, as seen in Fig. 2c–d. The color of LPF was lighter than SEF because there was much higher lignin content in SEF, as supported by the chemical composition analysis (Fig. 2e). The lignin residue in LPF was only 4.58 %, while the lignin content in SEF was as high as 32.19 %, FTIR spectra (Fig. 2d) further confirmed that, for example, the intensity of the absorption peaks at 1602 cm^{-1}, 1513 cm^{-1}, and 1460 cm^{-1} associated with aromatic skeletal vibrations of lignin was relatively stronger in SEF (Peng, Peng, Bian, Xu, & Sun, 2012; Wen, Xue, Xu, Sun, & Pinkert, 2013; Zuo et al., 2003). However, much more hemicellulose had degraded in the steam explosion method, hemicellulose residue was only 7.45 %. SEF had a little higher cellulose crystallinity (62.3 %) while cellulose crystallinity for LPF was 57.2 %.

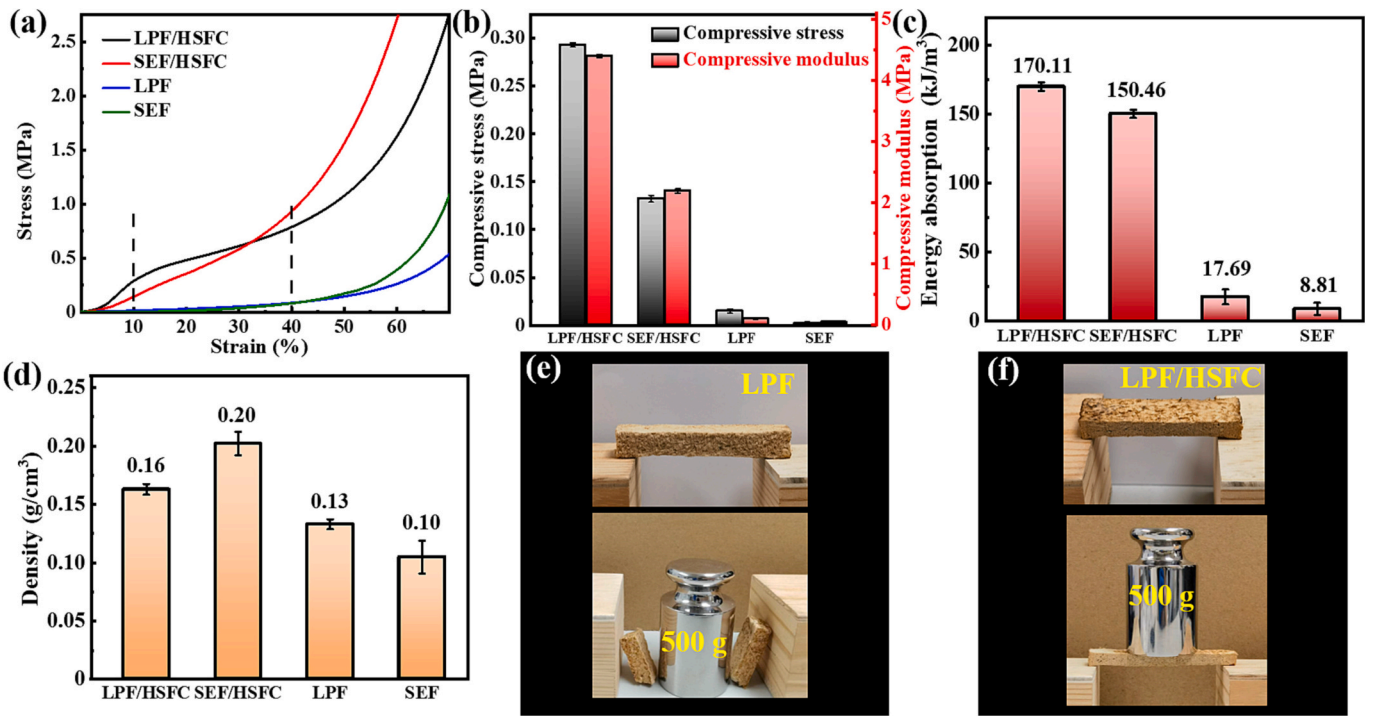

Fig. 5. Mechanical properties of bamboo fiber foams: (a) compressive stress-compressive strain curves, (b) compressive stress at 10 % strain and compressive modulus, (c) energy absorption capacity under 40 % strain, (d) density, (e) the breakage test of the LPF foam without HSFC, and breakage test of the LPF/HSFC foams.

Fig. 2h shows the AFM micrographs of the HSFC (solid content = 27 %) produced from mechano-enzymatic fibrillation at a high-consistency (35 wt%) approach, in which most pulp fibers were disintegrated into nanoscale fibrils but there was still a small fraction of fiber fragments and un-fibrillated microfibril bundles existing in the HSFC product. In this study, we thought that this type of not completely fibrillated HSFC material might be suitable as a natural "binder" to combine with relatively more coarse bamboo fibers to fabricate foams all derived from bamboo fibers.

3.2. Microstructure of bamboo fiber foams consisting of bamboo fibers and HSFC

Fig. 3 shows the difference in the internal microstructure of bamboo fiber foams using different bamboo fibers as a skeleton, meanwhile comparing the foam's microstructure with or without HSFC. With the HSFC incorporation, "film bridges" derived from the HSFC were generated as water evaporated, both ends of which adhered to the surface of bamboo fibers, thus enhancing the interaction among the fibers. In Fig. 3a–b, the skeletons of bamboo fibers and their porous structure were still clearly seen in the LPF/HSFC foam, while SEF skeletons were less evident in the SEF/HSFC foam due to a high degree of structural collapse occurring, as supported in Fig. S1, SEF/HSFC foam had a larger shrinkage rate (62.36 %) than LPF/HSFC foam (40.23 %), the fiber skeletons were wrapped by the HSFC. Bamboo fiber foams without the HSFC incorporation exhibited a much more loosely network structure (Fig. 3c–d), micro-sized bamboo fibers only simply assembled and interlaced with each other, and there were no evident contact points between adjacent fibers, as shown in the magnified SEM image (the insets in Fig. 3c–d). However, the HSFC alone without bamboo fibers was not able to give rise to a foam structure, as shown in Fig. S2, suggesting that bamboo fibers greatly contributed to the formation of the foams.

Fig. 4 displays the 2D micro-CT tomographs (black and white) of internal structures in different directions and the reconstructed three-dimensional (3D) structure (blue and white) of the foams consisting of bamboo fibers and HSFC. As seen in Fig. 4, there were numerous pores, indicated by the "black" part in micro-CT tomographs in x-y, x-z, and y-z planes, the "white" ones represented the composite structure consisting of fibers and HSFC to build the cell walls of the pores. The cell walls in the LPF/HSFC foam appeared thinner, finer, and more interconnective. The cellular structures in the LPF/HSFC foam appeared similar in three different x-y, x-z, and y-z planes, whereas the cell walls were thicker in the SEF/HSFC foam and appeared much different in three different planes. The cell walls in the SEF/HSFC foam seemed more disconnected, indicating that inhomogeneous cellular structures were formed when using the less uniform SEF bamboo fibers. The relatively coarse SEF with broader size distribution resulted in the formation of a more discontinued and bulk structure of cell walls, as seen in the micro-CT tomograph in Fig. 4b. By reconstructing a series of plane images into spatial configurations can build up a 3D structure model of bamboo fiber foams, as presented in Fig. 4d and j. The calculated porosity for LPF/HSFC foam and SEF/HSFC foam were 82.06 % and 74.02 %, respectively. There were more pores in the LPF/HSFC foam than in the SEF/HSFC foam, as simulated by the "white balls" inserted in the 3D reconstructed models, which represented the location and the size of pores in the foams. The size of the "white ball" varied depending on the actual pores, we can see "white balls" were relatively smaller, but the number of the "white balls" was relatively higher in the LPF/HSFC reconstructed model than in the SEF/HSFC one, as seen in Fig. 4d and h. To get insight into information regarding pore size distribution, the pore size distribution was further measured by a mercury method; the pore size distribution curves are displayed in Fig. S3. Most of the pore sizes for LPF/HSFC foam were about 30–500 μm, the peak of the size distribution was centered about 100 μm, while most of the pore sizes for SEF/HSFC foam were larger than 100 μm, and the peak of the size distribution was centered about 300 μm. Both foams had a small fraction of tiny pores with a size of about 3–8 μm.

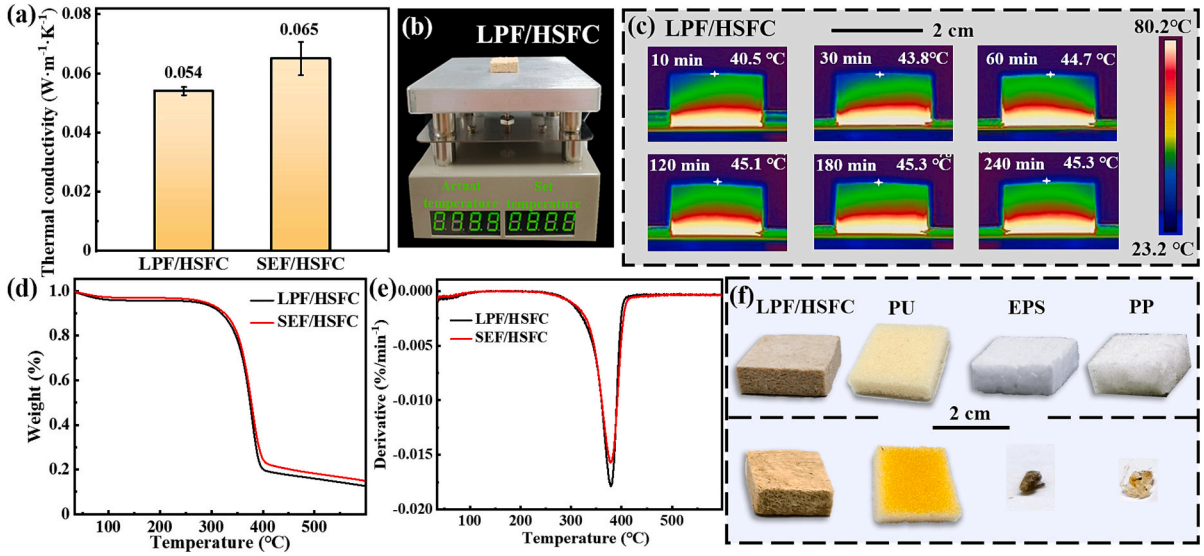

Fig. 6. Thermal stability and thermal insulation performance of bamboo fiber foams: (a) Thermal conductivity, (b) Photograph of the LPF/HSFC foam on a hot plate, (c) IR thermal imaging of the LPF/HSFC foam exposed to heating, (d) TG curves, (e) DTG curves and (f) photograph of bamboo fiber foams before and after 200 °C heating for 5 min on a hot plate in comparison with PU, EPS, PP.

3.3. Mechanical performance of bamboo fiber foams

Compressive performance is crucial to a wide range of applications. Fig. 5a shows the typical compressive stress-strain curves of bamboo fiber foams using two different types of bamboo fibers, meanwhile comparing the mechanical performance of the foams with or without HSFC. The stress-strain response for the LPF/HSFC foam exhibited a more noticeable three distinctive regions, which were common compressive deformation behaviors found in typical plastic foams. Namely, the first regions corresponded to linear elastic deformation before 10 % strain, which was largely due to elastic bending of cell edges and stretching of cell faces. The plateau occurred around 10 % ~ 40 % strain, referred to as the second region, largely because those cells maintained relatively constant yield stress by plastic deformation and cellular solid started bending or bucking, giving rise to a flat plateau region. The third region was the densification stage, in which most cells plastically collapsed, and the cell walls started to interact, therefore leading to a rapid increase in the stress from 40 % strain. As for the SEF/HSFC foam, the deformation of this foam exhibited a shear-thickening behavior under applied load, but the boundaries among the three stages were hard to distinguish. As mentioned previously in micro-CT tomograph analysis, there were more pores generated in the LPF/HSFC foam, and the cellular structure was relatively more consistent compared to those in the SEF/HSFC foam, this may explain why the deformation of the LPF/HSFC foam exhibited more noticeable three stages compared to the SEF/HSFC foam. LPF used as skeletons of the foam had a uniform size, which was beneficial for the formation of a relatively more uniform cellular structure (Fig. 4a).

As seen in Fig. 5b–c, the stress at 10 % strain and compressive modulus of the LPF/HSFC foams were 0.29 MPa and 4.40 MPa, respectively, compared to 0.13 MPa and 2.19 MPa for the SEF/HSFC foam. The LPF/HSFC foam significantly outperformed the SEF/HSFC foam concerning mechanical performance under the low strain range, although SEF/HSFC foam had a higher density (Fig. 5d) than LPF/HSFC foam. The relatively more regular and consistent cellular structure formed by uniform LPF could well distribute compressive stress and resist structural collapse, which may largely account for the superior mechanical performance of the LPF/HSFC foam over the SEF/HSFC foam. With the HSFC incorporation, the stress at 10 % strain for LPF/HSFC foam or SEF/HSFC foam was both one order of magnitude higher, and the compressive modulus was about 44-fold and 55-fold higher than the LPF foam and the SEF foam, respectively, suggesting the great mechanical reinforcing effect of nanocellulose in bamboo fiber foams. The "film bridges" generated from HSFC between fibers strengthened the interaction between adjacent fibers, thus enhancing physical entanglements among fibers, eventually leading to improved mechanical performance.

Energy absorption capacity is critical for applications such as protection packaging where shock absorption is needed to prevent failure. The energy absorption capacity at 40 % strain of LPF/HSFC and SEF/HSFC foams were as high as 170 kJ/m^3 and 150 kJ/m^3, respectively, compared to corresponding 17.69 kJ/m^3 and 8.81 kJ/m^3 for those without nanocellulose. The result suggested the superior energy absorption capacity of foams obtained with the incorporation of nanocellulose. As displayed in the breakage test in Fig. 5e–f, the stick of the LPF foam without the nanocellulose reinforcement easily broke apart when a 500 g weight was placed on top of the stick. Similar phenomenon was also reported in the literature that the lignocellulosic foams without external natural or synthetic chemical binders generally had poor mechanical properties because of the lack of sufficient interaction among lignocellulosic fibers. However, the LPF/HSFC foam stick was able to hold a 500 g load without breaking, indicating that the incorporation of HSFC as a reinforcement greatly strengthened the bamboo fiber foams by enhancing the interconnection and interactions between the adjacent fibers to make foam more structural integrity, increasing its capacity to enable to withstand external forces.

3.4. Thermal insulation performance and thermal stability of bamboo fiber foams

The LPF/HSFC foam possessed low thermal conductivity (about 0.054 W/(m•K)), which was lower than that of the SEF/HSFC foam (about 0.065 W/(m•K)) because LPF/HSFC had high porosity as discussed previously. Fig. 6b–c shows that the LPF/HSFC foam was heated on a hot plate (80 °C) and the infrared thermal images were captured at various time intervals. The surface temperature of the foam on the side far from the hot plate increased with the increase of the heating exposure time, but the increase in the temperature became very slow and stabilized after 1 h, the surface temperature was still kept low after 4-h heating exposure as seen from the infrared thermal images (Fig. 6c). Thermal stability of natural or plastic foams is critical for guaranteeing their long-term service in their practical applications under variable

Table 1
Mechanical performance and thermal insulating property of other lignocellulosic foams.

Foam type	Drying method & time	Density (g/cm^3)	Compressive strength (MPa)	Compressive modulus (MPa)	Energy absorption (kJ/m^3)	Thermal conductivity (W/(m•K))	Reference
Thermomechanical pulp filled with 5 % cellulose nanofibers	Microwave radiation & 3–8 min	0.10–0.20	0.09–0.035 at 10 % strain	0.85–5.70	–	0.045–0.070	(Hafez & Tajvidi, 2021)
Dissolved cellulose (cotton filter pulp) in urea/NaOH with 10 % bentonite	Ambient drying & –	0.09	–	39.4	–	0.063	(Chen et al., 2022)
Disc milled pretreated chemi-thermomechanical pulp with sodium dodecyl sulfate (0.6 g/L) as foaming agent	Ambient drying & 10 h	~0.01	0.02–0.03 at 80 % strain	0.015–0.020	4–5 under 80 % strain	0.031–0.033	(Zhu et al., 2022)
Bamboo pulp fibers filled with nanocellulose via liquid phase exchange route	Ambient drying & –	0.08–0.12	–	0.49–2.96	40–110 under 40 % strain	0.0368–0.0466	(Sun et al., 2023)
Eucalyptus pulp cellulose pulp suspension	Thermal drying & 12 h	0.06–0.12	0.02–0.11	0.18–1.20	–	0.03–0.04	(Lujan, Goñi, & Martini, 2022)
Microfibrillated refiner mechanical pulp fibers with clay and olefin sulfonate	Thermal drying (75 °C) & 6 h	0.136	0.126 at 25 % strain	0.805	–	0.043	Zhu et al., 2023
Lignin-containing pulp fibers (LPF) filled with HSFC	Thermal drying (200 °C) & 1.5 h	0.16	0.29 at 10 % strain	4.4	170 under 40 % strain	0.054	This work

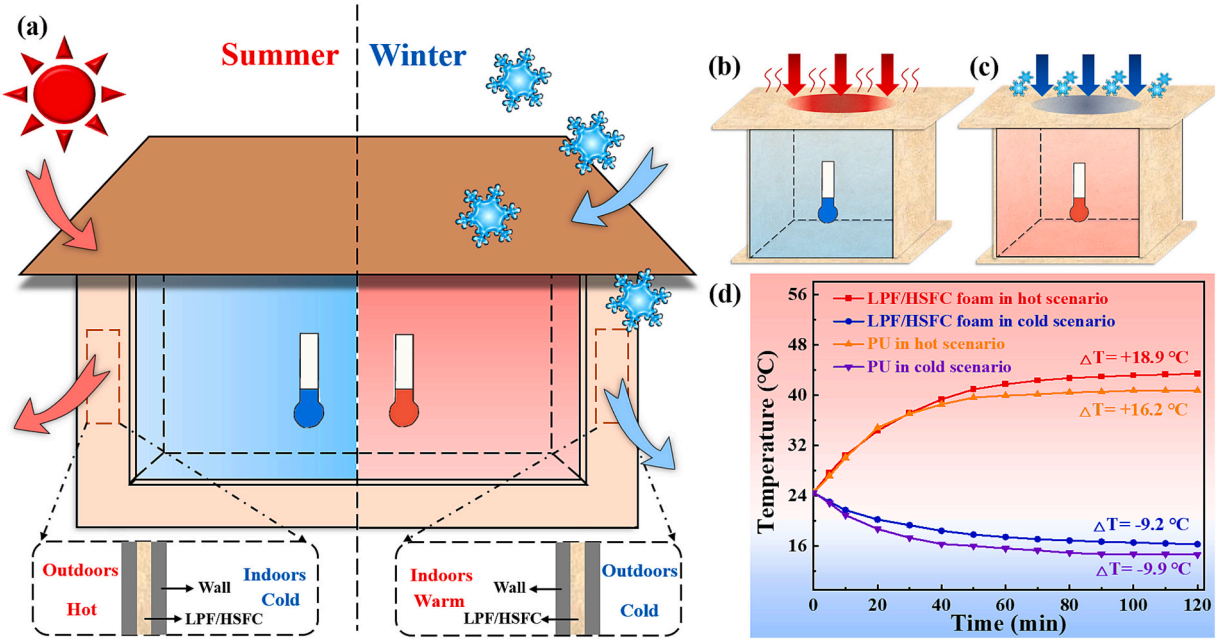

Fig. 7. (a) The scenario of bamboo fiber foams as thermal insulating materials in a bungalow building; (b) schematic diagram of the model bungalow in a hot scenario, (c) schematic diagram of the model bungalow in a cold scenario and (d) the comparison of temperature change using the LPF/HSFC foam as thermal insulating materials and PU in the model bungalow under hot and cold scenarios within 120 min.

temperatures. The thermal stability of the bamboo fiber foams was evaluated by TG and DTG analyses, their corresponding typical TG curves and DTG curves of the LPF/HSFC foam and SEF/HSFC foam are displayed in Fig. 6d–e, respectively. Regardless of which type of bamboo fibers was used as skeletons in the foams, both bamboo fiber foams exhibited similar thermal degradation behavior. A small fraction of weight loss occurred at around 100 °C, which was ascribed to the removal of water residues in the foams. The fibers or nanocellulose in the foams started to decompose as temperature further increased, the onset degradation temperature was around 345 °C, and the major degradation with about 80 % weight loss for the LPF/HSFC foam was from 250 to 400 °C, which was largely attributed to the thermal decomposition of cellulose and hemicellulose (Chen et al., 2022). The thermal stability of bamboo foams was further compared with some common plastic foams such as PP, EPS, and PU by directly placing them on a hot plate set at 200 °C. As the time of heating elapsed, except for PU foam, other plastic foams gradually shrunk, and eventually deformed dramatically, as demonstrated in Fig. 6f. There was almost no obvious thermal shrinkage and structure collapse for the developed bamboo fiber foams in this study, indicating their superior thermal stability than most petrochemical-based foams.

Compared to the mechanical- and thermal insulation performances of cellulosic-based foams developed by other research groups as summarized in Table 1. The LPF/HSFC foams developed in this study possessed high production efficiency and integrated performances in terms of mechanical properties, thermal insulation performance, and good thermal stability. Therefore, the LPF/HSFC foams and PU foams were used as thermal insulating materials that were installed in all

directions and simulated for use in the thermal insulating building, as demonstrated in Fig. 7a. In the hot scenario, when exposed to heat sources, the interior temperature of the testing chamber made of all LPF/HSFC materials gradually increased to 43.4 °C from 24.5 °C after 120 min, and then the plateau started. The indoor temperature of the PU building model gradually increased to 40.7 °C from 24.5 °C after 120 min. In the cold scenario, the indoor temperature with the LPF/HSFC foams as thermal insulating materials gradually decreased from 24.5 °C to 16.3 °C after 120 min and then stabilized. The indoor temperature inside the building model using PU as thermal insulating materials gradually decreased from 24.5 °C to 14.6 °C after 120 min, suggesting that the developed LPF/HSFC foams have similar or comparable insulation performance as some commercial PU foams. Besides thermal insulation performance, LPF/HSFC had comparable mechanical performance and energy absorption capability as commercial PU, but PU had a lower density, as shown in Figs. S4 and S5.

4. Conclusions

In summary, we developed a facile and efficient approach to construct a bamboo fiber foam fully derived from natural sources (i.e., bamboo fibers and HSFC) through high temperature drying. It was found that the HSFC incorporation endowed the bamboo fiber foams with excellent mechanical robustness and mechanical energy absorption capacity, showing nearly one order of magnitude higher stress at 10 % strain and mechanical energy absorption compared to those without the HSFC. Moreover, the compressive modulus of the LPF/HSFC and the SEF/HSFC foams increased 44 times and 55 times, respectively. The LPF has proven to be more suitable to be used as a skeleton than SEF for constructing bamboo fiber foams, yielding the foams with higher mechanical and thermal insulation performance because of the formation of a more regular cellular structure by a much more uniform size and shape of LPF. The LPF/HSFC foams possessed good thermal insulation properties with a thermal conductivity of 0.054 W/(m•K) and exhibited excellent thermal stability as well as excellent mechanical performances and energy absorption capacity, suggesting that this type of bamboo fiber foam obtained in this study holds promise for use in protective packaging under extremely hot environments or buildings for thermal insulation.

CRediT authorship contribution statement

Xin Li: Writing – original draft, Investigation, Formal analysis, Data curation. **Tuhua Zhong:** Writing – review & editing, Supervision, Methodology, Funding acquisition, Conceptualization. **Yunyan Xiao:** Investigation, Formal analysis. **Haitao Cheng:** Writing – review & editing, Funding acquisition. **Hong Chen:** Writing – review & editing, Supervision, Methodology, Funding acquisition, Conceptualization.

Declaration of competing interest

The authors declare that they have no known competing financial interests or personal relationships that could have appeared to influence the work reported in this paper.

Data availability

Data will be made available on request.

Acknowledgments

This work was supported by the National Key Research & Development Program of China (2023YFD2202102 and 2022YFD2200901) and the Fundamental Research Funds of the International Centre for Bamboo and Rattan (ICBR) (1632021025).

Appendix A. Supplementary data

Supplementary data to this article can be found online at https://doi.org/10.1016/j.carbpol.2024.121966.

References

Ates, M., Karadag, S., Eker, A. A., & Eker, B. (2022). Polyurethane foam materials and their industrial applications. *Polymer International, 71*(10), 1157–1163.
Blettler, M. C., Ulla, M. A., Rabuffetti, A. P., & Garello, N. (2017). Plastic pollution in freshwater ecosystems: Macro-, meso-, and microplastic debris in a floodplain lake. *Environmental Monitoring and Assessment, 189*, 1–13.
Chen, L., Wang, S., Wang, S., Chen, C., Qi, L., Yu, L., Lu, Z., Huang, J., Chen, J., Wang, Z., Shi, X., Song, Z., Liu, H., & Chen, C. (2022). Scalable production of biodegradable, recyclable, sustainable cellulose - Mineral foams via coordination interaction assisted ambient drying. *ACS Nano, 16*(10), 16414–16425.
Ferreira, E., Cranston, E., & Rezende, C. (2020). Naturally hydrophobic foams from lignocellulosic fibers prepared by oven-drying. *ACS Sustainable Chemistry & Engineering, 8*(22), 8267–8278.
Gupta, P., Singh, B., Agrawal, A. K., & Maji, P. K. (2018). Low density and high strength nanofibrillated cellulose aerogel for thermal insulation application. *Materials & Design, 158*, 224–236.
Hafez, I., & Tajvidi, M. (2021). Comprehensive insight into foams made of thermomechanical pulp fibers and cellulose nanofibrils via microwave radiation. *ACS Sustainable Chemistry & Engineering, 9*(30), 10113–10122.
Jaxel, J., Markevicius, G., Rigacci, A., & Budtova, T. (2017). Thermal superinsulating silica aerogels reinforced with short man-made cellulose fibers. *Composites Part A: Applied Science and Manufacturing, 103*, 113–121.
Jiménez-Saelices, C., Seantier, B., Cathala, B., & Grohens, Y. (2017). Spray freeze-dried nanofibrillated cellulose aerogels with thermal superinsulating properties. *Carbohydrate Polymers, 157*, 105–113.
Li, P., Wang, X., Su, M., Zou, X., Duan, L., & Zhang, H. (2021). Characteristics of plastic pollution in the environment: A review. *Bulletin of Environmental Contamination and Toxicology, 107*, 577–584.
Liu, Y., Lu, P., Xiao, H., Heydarifard, S., & Wang, S. (2017). Novel aqueous spongy foams made of three-dimensionally dispersed wood-fiber: Entrapment and stabilization with NFC/MFC within capillary foams. *Cellulose, 24*, 241–251.
Lujan, L., Goñi, M. L., & Martini, R. E. (2022). Cellulose-chitosan biodegradable materials for insulating applications. *ACS Sustainable Chemistry & Engineering, 10*(36), 12000–12008.
Ma, S., Liu, C., Xu, Y., Wang, L., Wang, H., Xu, W., Zhuang, Y., & Yang, H. (2021). Bioinspired cellulose foam with excellent water wicking and flux properties prepared using ice template. *The Journal of Physical Chemistry B, 125*(22), 5853–5861.
Malekzadeh, H., Md Zaid, N., & Bele, E. (2021). Characterization and structural properties of bamboo fibre solid foams. *Cellulose, 28*, 703–714.
Markevicius, G., Ladj, R., Niemeyer, P., Budtova, T., & Rigacci, A. (2017). Ambient-dried thermal superinsulating monolithic silica-based aerogels with short cellulosic fibers. *Journal of Materials Science, 52*, 2210–2221.
Moon, R. J., Martini, A., Nairn, J., Simonsen, J., & Youngblood, J. (2011). Cellulose nanomaterials review: Structure, properties and nanocomposites. *Chemical Society Reviews, 40*(7), 3941–3994.
Peng, P., Peng, F., Bian, J., Xu, F., & Sun, Y. C. (2012). A comparative study of bamboo (Phyllostachys incarnata Wen) milled wood lignin and the successively alkali-fractionated lignins. *Wood Science and Technology, 46*, 871–885.
Pere, J., Tammelin, T., Niemi, P., Lille, M., Virtanen, T., Penttila, P. A., … Gronqvist, S. (2020). Production of high solid nanocellulose by enzyme-aided fibrillation coupled with mild mechanical treatment. *ACS Sustainable Chemistry & Engineering, 8*(51), 18853–18863.
Segal, L., Creely, J. J., Martin, A. E., Jr., & Conrad, C. M. (1959). An empirical method for estimating the degree of crystallinity of native cellulose using the X-ray diffractometer. *Textile Research Journal, 29*(10), 786–794.
Sluiter, A., Hames, B., Ruiz, R., Scarlate, C., Sluiter, J., Templeton, D., & Crocker, D. (2008). Determination of structural carbohydrates and lignin in biomass. *Laboratory Analytical Procedure, 1617*(1), 1–16.
Sun, L., Liu, L., Wu, M., Wang, D., Shen, R., Zhao, H., Lu, J., & Yao, J. (2023). Nanocellulose interface enhanced all-cellulose foam with controllable strength via a facile liquid phase exchange route. *Carbohydrate Polymers, 299*, Article 120192.
Sun, Y., Chu, Y., Wu, W., & Xiao, H. (2021). Nanocellulose-based lightweight porous materials: A review. *Carbohydrate Polymers, 255*, Article 117489.
Turner, A., & Lau, K. S. (2016). Elemental concentrations and bioaccessibilities in beached plastic foam litter, with particular reference to lead in polyurethane. *Marine Pollution Bulletin, 112*(1–2), 265–270.
Vethaak, A. D., & Legler, J. (2021). Microplastics and human health. *Science, 371*(6530), 672–674.
Wang, J., Xu, H., Zhang, Y., Dai, F., Wang, Z., Wang, H., & Zhong, T. (2022). Morphology, structure and property of high consistency mechano-enzymatic fibrillated cellulose: Effect of treatment consistency of bamboo pulp fibers. *Industrial Crops and Products, 188*, Article 115731.
Wang, X., Zhang, Y., Jiang, H., Song, Y., Zhou, Z., & Zhao, H. (2016). Fabrication and characterization of nano-cellulose aerogels via supercritical CO_2 drying technology. *Materials Letters, 183*, 179–182.
Wen, J. L., Xue, B. L., Xu, F., Sun, R. C., & Pinkert, A. (2013). Unmasking the structural features and property of lignin from bamboo. *Industrial Crops and Products, 42*, 332–343.

Wu, G., Xie, P., Yang, H., Dang, K., Xu, Y., Sain, M., Turng, L., & Yang, W. (2021). A review of thermoplastic polymer foams for functional applications. *Journal of Materials Science, 56*, 11579–11604.

Wu, J., Zhong, T., Zou, Y., Li, J., Zhao, W., & Chen, H. (2023). Microstructure, chemical composition and thermal stability of alkali-treated bamboo fibers and parenchyma cells: Effects of treatment time and temperature. *Cellulose, 30*(3), 1911–1925.

Wu, M., Yu, G., Chen, W., Dong, S., Wang, Y., Liu, C., & Li, B. (2022). A pulp foam with highly improved physical strength, fire-resistance and antibiosis by incorporation of chitosan chitosan and CPAM. *Carbohydrate Polymers, 278*, Article 118963.

Zhao, W., Zhao, H., Cheng, J., Li, W., Zhang, J., & Wang, Y. (2022). A green, durable and effective flame-retardant coating for expandable polystyrene foams. *Chemical Engineering Journal, 440*, Article 135807.

Zhu, Y., Zhu, J., Li, Y., Chen, J., Rojas, O., & Jiang, F. (2023). Chemical binder-free and oven-dried lignocellulose/clay composite foams: Flame resistance, thermal insulation, and recyclability. *ACS Sustainable Chemistry & Engineering, 11*(46), 16499–16508.

Zhu, Y., Zhu, J., Yu, Z., Ye, Y., Sun, X., Zhang, Y., Zhu, P., & Jiang, F. (2022). Air drying scalable production of hydrophobic, mechanically stable, and thermally insulating lignocellulosic foam. *Chemical Engineering Journal, 450*, Article 138300.

Zuo, S., Gao, S., Yuan, X., & Xu, B. (2003). Carbonization mechanism of bamboo (*phyllostachys*) by means of Fourier Transform Infrared and elemental analysis. *Journal of Forestry Research, 14*(1), 75–79.